doi:10.2533/chimia.2015.729 Chimia 69 (2015) 729–733

Electrode Engineering of Conversion-based Negative Electrodes for Na-ion Batteries

Leonie O. Vogt, Cyril Marino, and Claire Villevieille*

Abstract: Due to lower costs and higher abundance of sodium, Na-ion battery technology can offer a good alternative to Li-ion batteries. Much research is focusing on developing new cathode and anode materials but the importance of the electrode engineering on the electrochemical performance is often neglected. The electrode composition is especially crucial for conversion reaction-based materials where the composite electrode (active material, conducting additive and binder) has to buffer the huge volume change occurring upon cycling. This work highlights the differences observed on Sn-CMC electrode performance by using different Sn particle sizes (micro- and nanoparticles) and evaluating the role of the conductive additive in the electrode. Carbon fibers (VGCF) demonstrate a good ability to surround micrometer particles but not especially nanometer particles leading to an improvement in the performance of microparticles but not of nanoparticles. For a high loading electrode suitable for full cell applications (>3.5 mg/cm^2 of active material), nanometer particles show limited performance for long-term cycling. The combination of VGCF with micrometer particles seems to be the most promising composition to obtain good performances for conversion reaction based-materials.

Keywords: Electrode engineering · Na-ion batteries · Negative electrode · Sn particle · VGCF

Li-ion batteries are starting to reach their limits in terms of energy density, cost, and abundance, and progress is slower than expected. Thus, researchers are currently re-investigating other alkali metals as Li substitutes, mainly focusing on Na. This system has been considered to be purely academic, and no real applications or prototypes have been developed to investigate its viability or possible commercialization, the only exception being the high temperature Na-S system, which was commercialized in the 1960s.[1] Recently however, the amount of research and number of papers devoted to the development of active materials for Na-ion batteries has increased exponentially, leading the community to consider the commercialization of Na-ion batteries in the near future.[2–6] Electrochemically, specifically voltage and theoretical specific charge, there is no advantage to replacing Li with Na. However, when considering additional parameters such as abundance and cost, Na-ion batteries may be competitive with the currently available Li-ion batteries. Another significant advantage in terms of both cost and weight is that no alloy exists between sodium and aluminum. This means that Al can be used as a cheaper current collector for both the positive and negative electrodes, lowering the total weight and cost of the cell pack. Furthermore, the electrolyte in Na-ion batteries has a higher conductivity compared to that of Li-ion batteries. The larger ionic radius of Na compared with Li results in a low de-solvation energy, which strongly influences the kinetics and allows high power Na-ion batteries to be envisaged. To achieve commercialization, suitable anodes[2,4,7–11] and cathodes[12–21] must be developed and studied in depth as the Na-system is often not analogous to the Li-system. A couple of years ago, the observation that pure commercial elements, such as Sn or Sb can electrochemically react with Na, leading to sustainable reversible capacities as high as 500 mAh/g over more than 100 cycles (twice as much as hard carbon), surprised the scientific community.[7,22] These results were especially interesting considering the immense volume change upon cycling, which exceeds 400%. However, while the search for new materials is progressing rapidly, the engineering of the electrodes is quite often neglected. Many groups in the literature reported as an example that polyvinylidene fluoride binder (PVDF) works poorly in Na-ion batteries and that other type of binders should be used instead.[23–25] We were one of the first groups to demonstrate that the know-how acquired over the past few decades on Li-ion battery technology cannot be transferred one-to-one to the emerging Na-ion batteries.[26] In fact, we demonstrated that the most commonly used binder in Li-ion batteries (PVDF) is not suitable for Na-ion batteries as it decomposes to create NaF during cycling and thus the electrode loses its integrity and cannot accommodate the volume change of the conversion-based electrode materials anymore.[26] Besides the binder, carbon-conductive agents (carbon fibers, super P, acetylene black, carbon nanotubes, *etc.*) are another source of variation from group to group, where many different types are used but it is difficult to establish which of them leads to the best cycling performance with conversion-based electrode materials for Na-ion batteries.[27–29]

The influence of the particle size (of the active material) is another often neglected factor in literature, since articles either focus on nanoparticles or they focus on solid-state bulk particles (tens of µm range). The comparison between both particle sizes (nano and micro range) is not often reported and it is difficult to assess the advantages and drawbacks of each since the loading of the electrodes (using either nano or micro range) can differ by a factor of 5 to 10.[9,30–33] Based on the common approach of using very low loading for nanoparticle active materials (unsuitable

*Correspondence: Dr. C. Villevieille
Paul Scherrer Institut
Electrochemistry Laboratory
CH-5232 Villigen PSI
E-mail: Claire.villevieille@psi.ch

for battery application) it is not surprising that nanoparticles are often presented to be better in terms of cycling stability, long-term cycling and power performance, as for example reported recently by Nam *et al*.[34] and others.[35–39]

In this article, we establish an engineering guideline for conversion-based negative electrodes used in Na-ion batteries. Sn was selected as a model conversion-based material that undergoes high volume changes during cycling. Due to the instability of the PVDF binder in Na-ion batteries, shown previously, it was decided to use the promising binder Na-CMC. Here we compare the impact of different particle sizes on the electrochemical performance in electrodes of comparable loading. Additionally, we investigate the impact of the carbon conductive agent in both the microparticle and the nanoparticle systems, looking specifically at the use and impact of carbon Super C and carbon fiber. The best combination of binder/conductive additive/particle size for improved cycling performance of conversion-based negative electrodes in Na-ion batteries is then elucidated.

Experimental Section

Electrode Preparation

For the electrode preparation we used two different tin powders: Sn-micro (ABCR, 325 mesh) (hereafter called m-Sn) and Sn-nano (ABCR, *ca.* 100 nm, hereafter called n-Sn). For the conductive agent, two different types were used: carbon black SuperC65 (CB, Imerys) and vapor-grown carbon fibers (VGCF, Showa Denko). Electrodes without VGCF were prepared by casting a suspension of 70 wt% Sn-micro (or Sn-nano), 18 wt% CB and 12 wt% carboxymethyl cellulose sodium salt (CMC, Alfa Aesar) in deionized water onto aluminum foil, used as current collector (described in the article as composition 1). For electrodes containing VGCF, the ratio between the elements was modified to 70 wt% Sn-micro (or Sn-nano), 9 wt% CB, 9 wt% VCGF and 12 wt% CMC (described in the article as composition 2). Once dried in air, 13 mm diameter electrodes were punched out and were dried under vacuum at 120 °C for a few hours. The loading of active material on the electrodes was between 2.8 mg/cm^2 and 3.5 mg/cm^2.

Electrochemistry

Electrochemical cells were assembled in an Ar-filled glove box using the electrode, a glass-fiber sheet as the separator and metallic sodium (Sigma-Aldrich, 75 μm) as counter electrode. A mixture of 1 M $NaClO_4$ dissolved in propylene carbonate (PC) was used as electrolyte. The cell performance was measured in galvanostatic mode at 25 °C between 5 mV and 1.0 V at a C/30 rate and monitored by an ASTROL cycling device. An additional potentiostatic step of 2h was added at the end of each discharge and charge to ensure proper sodiation and desodiation. All the potentials mentioned in the manuscript are given versus Na^+/Na.

Scanning Electron Microscopy (SEM)

SEM measurements were performed in a Carl Zeiss Ultra55 scanning electron microscope using the secondary electron mode.

Results and Discussion

Influence of Particle Size

The SEM pictures of m-Sn and n-Sn electrodes are displayed in Fig. 1 and show the impact of the particle size on the electrode engineering. The m-Sn electrode reveals a broad range of particle sizes from *ca.* 1 μm to 15 μm. Some Sn particles are close to each other and in other areas there are big gaps, indicating a certain inhomogeneity at the micrometer range in the dispersion of the particles in the electrode. The images also show some Sn particles that are only partially covered by the carbon Super C and the CMC binder and some cracks around the particles. Those fractures occurring in the electrode can be problematic considering the huge volume change occurring during the sodiation of Sn particles (especially for the m-Sn electrode). Particles that are only partially connected to the carbon/binder/current collector are likely to be totally disconnected during the cycling due to the strong strain caused by the volume change upon sodiation. This phenomenon would lead to a decrease of the cell performance. The n-Sn electrode shows a narrow particle size distribution since the Sn particles are below 500 nm, with most of them around 100 nm diameter. At low magnification (micrometer range SEM picture, Fig. 1, bottom), the Sn nanoparticles seem to be well dispersed and embedded in the carbon/binder matrix unlike the m-Sn electrode. Thus, upon cycling versus Na the nanoparticle system is expected to accommodate the volume expansion better than the microparticle system. However, the picture taken at higher magnification (Fig. 1, bottom) reveals some n-Sn agglomerates, indicating that the electrode engineering could be optimized further. This agglomeration of nanoparticles may be a result of the high nanoparticle loading used here, as compared to the low loading generally reported in literature. In both cases, the images also indicate a good porosity such that the wettability of the electrode should not be a cause of fading.

Fig. 2 depicts the cycling performance of m-Sn and n-Sn in electrode composition 1. The specific charge of the m-Sn is constantly decreasing along cycling. The specific charge starts at the first cycle with a value close to 800 mAh/g and drops down to reach only 300 mAh/g after 20 cycles. Additionally, it is noteworthy that the difference between the charge and the discharge is very low, indicating a good Coulombic efficiency. For the n-Sn, the results are different with a similar specific charge for the first cycle at around 750 mAh/g, and stabilization over six cycles at a specific charge of 650 mAh/g. After six cycles, the specific charge collapses dramatically to reach only 50 mAh/g after 20 cycles. The

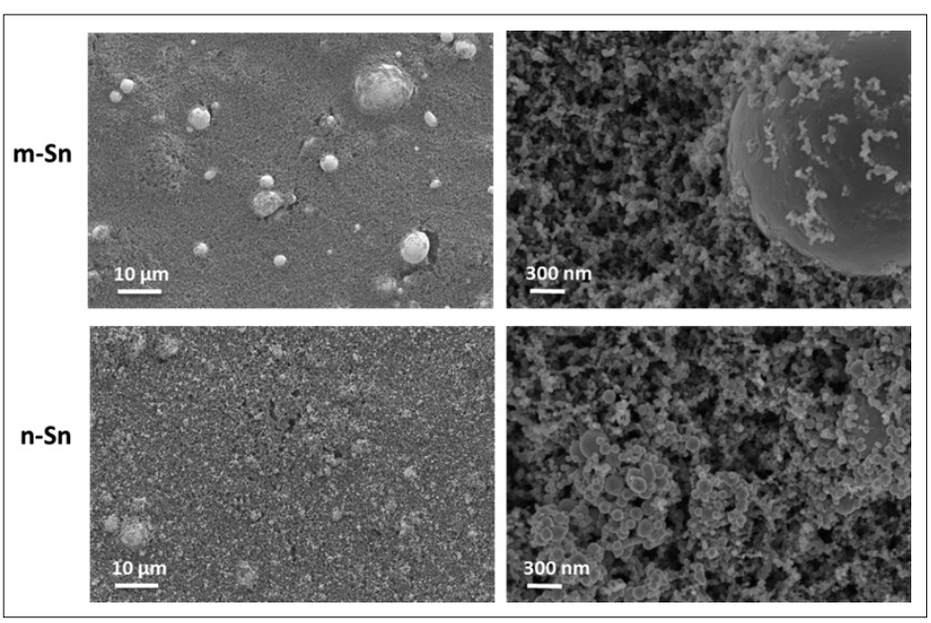

Fig. 1. SEM images of m-Sn-micro (top) and n-Sn electrodes (bottom) in electrode composition 1.

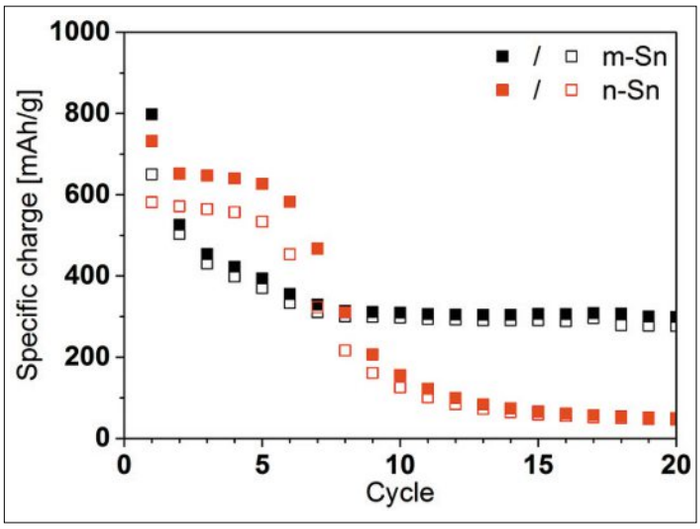

Fig. 2. Cycling performance obtained for m-Sn and n-Sn in composition 1.

Coulombic efficiency in the case of n-Sn is relatively low compared to the m-Sn.

The difference observed between the two electrodes m-Sn and n-Sn can be explained by the difference in particle size. The nanoparticles have such high surface area that when cycling in a potential window where the electrolyte is reduced, more electrolyte decomposition occurs and consequently more solid electrolyte interphase (SEI) forms, leading to a low Coulombic efficiency. With every cycle the SEI layer is thickened, its isolating character leads to an increased resistance which finally hinders cyclability. For the m-Sn the fading is mainly caused by the particle fracture which occurs during sodiation. In fact when fully sodiated the particles expand 420%, leading to cracking which can cause loss of electrical contact of some particles. Those parts become dead materials that cannot cycle anymore, leading to a gradual fading of specific charge. These results are in accordance with the SEM observations and predictions, in that m-Sn was seen to integrate less well in the carbon/binder matrix than n-Sn (Fig. 1) and consequently it is more likely to suffer from pulverization and electrical disconnection of particles, leading to gradual specific charge fading as seen in Fig. 2. However compared to the n-Sn electrode, the m-Sn electrode has a better specific charge after 20 cycles, coming from the fact that during cycling most probably after each fracture of the particle, a core-shell process is occurring and thus 'new-fresh' Sn can be revealed and can be cycled, which helps to maintain the specific charge higher than the isolating n-Sn.

The galvanostatic curves presented in Fig. 3 validate our hypothesis about the SEI formation in the n-Sn system. At *ca.* 0.4 V during the first sodiation a long potential plateau ascribable to the SEI formation is visible in the n-Sn sample whereas almost nothing appears in the same voltage range for the m-Sn electrode.

For the rest of the first sodiation, we can see the three characteristic potential plateaus of Na-Sn alloys at 0.2 V, 0.07 V and 0.01 V. For the n-Sn electrode, those potential plateaus are slightly lower in potential, indicating a higher polarization. This higher polarization probably arises from the larger SEI formation which hinders the lowest sodiation plateau to be accessed since with the additional overpotential it lies below the 5 mV cut-off voltage. On desodiation, a first potential plateau appears in the m-Sn electrode at 0.16 V but no such potential plateau is seen for the n-Sn electrode. Thereafter the desodiation plateaus of the n-Sn electrode (0.27 V and 0.54 V) are analogous to those of the m-Sn electrode (0.26 V and 0.53 V), with the slight shift in potential being attributable to the higher polarization in the n-Sn system (thicker SEI).

At the 10th cycle (Fig. 3, right), the polarization has grown in both electrodes such that the lowest potential plateau is no longer accessible for both systems. In general the different potential plateaus on sodiation are no longer distinguishable for m-Sn electrode and for the n-Sn electrode only two vague potential plateaus are visible at *ca.* 0.3 V and *ca.* 40 mV. In contrast, on desodiation potential plateaus are still distinguishable for both m-Sn and n-Sn allowing some comparison to the first cycle. For m-Sn the two potential plateaus at 0.27 V and 0.54 V are the most prominent features but have shortened in comparison to the 1st cycle. For n-Sn a new, small potential plateau is seen at 0.22 V followed by one at 0.28 V. Then the potential increases rapidly with a small bend at 0.55 V and another at 0.81 V.

So far we demonstrated that when the loading of the electrodes is the same, nanoparticles do not outperform microparticles after a few cycles. Instead, n-Sn shows a poor Coulombic efficiency and a dramatic specific charge fading. Nanoparticles can only compete with microparticles if the loading is low. However, due to the limited storage capacity such low loading is not commercially viable. A similar comparative approach was used to investigate the most suitable conductive agent and optimal electrode engineering conditions for the best electrochemical performances.

Influence of Conductive Additive

SEM pictures of the electrode designed with VGCF are shown in Fig. 4 and can be compared with the one having only Super C as a conductive additive (Fig. 1). The VGCF, a long rod shape of around 100 nm diameter, can easily be distinguished in composition 2. For both particle sizes, the observations made previously about the dispersion of Sn particles in Super C-based electrodes are also valid for VGCF-based electrodes: the micrometer particles are not homogeneously distributed in the electrode and the nanometer particles agglomerate slightly. The new electrode constituent, VGCF, shows a homogeneous dispersion throughout the electrode. For m-Sn VGCF electrodes, the Sn particles are covered by the VGCF (Fig. 4), such that electrode fractures around the micro Sn particles are bridged by the fibers. This is expected to lead to better electrical contact in the electrode during cycling. For the n-Sn, the situation is slightly different since the diameter of the VGCF is roughly the same as the one of the primary

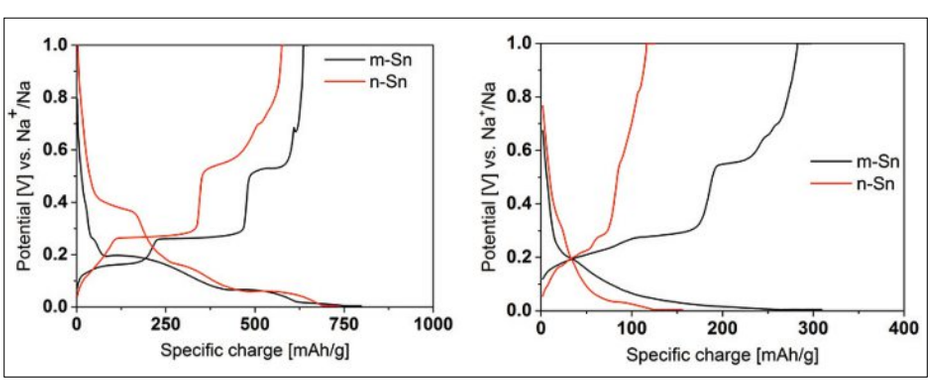

Fig. 3. Galvanostatic curves for the 1st (left) and 10th (right) cycle for the m-Sn and n-Sn electrodes.

particles. The interaction between the n-Sn particles and the VGCF is therefore limited and VGCF mainly serves to connect aggregates.

Looking now at composition 2 (with VGCF, Fig. 5), we can see that the trend between m-Sn and n-Sn is roughly the same as the one observed for composition 1. While the composition 2 does not seem to affect cycling for n-Sn, for m-Sn it increases and helps to maintain the specific charge. As already stated before for m-Sn, when particle fracture occurs upon sodiation, this can lead to some particles becoming disconnected leading to uncyclable material. Due to their length and high conductivity carbon fibers can combat this problem, allowing more Sn particles to stay connected to the carbon/binder matrix and current collector, which leads to a higher specific charge retention (*ca.* 400 mAh/g after 20 cycles). In n-Sn electrodes where the particles are well integrated and disconnection is not a problem but instead a thick SEI layer causes trouble, the addition of VGCF does not improve cycling performance.

This demonstrates that it is crucial to understand the cause of capacity fading and use the appropriate electrode engineering to combat the drawbacks of the active material. The VGCF improves the long-term cycling performance of the m-Sn electrode due to better electrical contact. However, there is a small cost in Coulombic efficiency due to SEI formation on the surface of the carbon fibers. For n-Sn, where thick SEI formation leads to dramatic specific charge fading, VGCF cannot help but instead, a coating of the Sn particles may help to reduce electrolyte decomposition to improve long-term performance. The galvanostatic curves of m-Sn for the 1st and 10th cycle in composition 1 and composition 2 are shown in Fig. 6. In the first cycle, a new feature at *ca.* 0.42V for the composition 2 electrode can be seen. This extra 'bump' is most probably due to the SEI formation at the surface of the VGCF leading to a slightly reduced Coulombic efficiency as previously mentioned. We notice a similar plateau in the n-Sn galvanostatic curve for the composition 1. The addition of VGCF to the electrode composition reduces the overpotential compared to the standard Super C electrode, which is seen by the different Na-Sn sodiation potential plateaus all lying at slightly higher potential.

This means that the lowest of the three characteristic tin sodiation potential plateaus at 0.01 V is fully accessible which leads to a higher specific charge for composition 2. On desodiation the curves obtained with composition 2 are analogous to the ones of composition 1 except that the potential plateau at *ca.* 0.16 V, which corresponds to the lowest potential plateau in sodiation, is longer.

At the 10th cycle, features observed on sodiation have merged into sloping curves for electrode composition 1 and electrode composition 2. As already observed with composition 1, on desodiation the different potential plateaus are still distinguishable. With composition 1, the lowest potential plateau at 0.16 V is no longer visible, however, with composition 2 an activity is still present at this potential. At *ca.* 0.28 V both compositions show a potential plateau, however with composition 2,

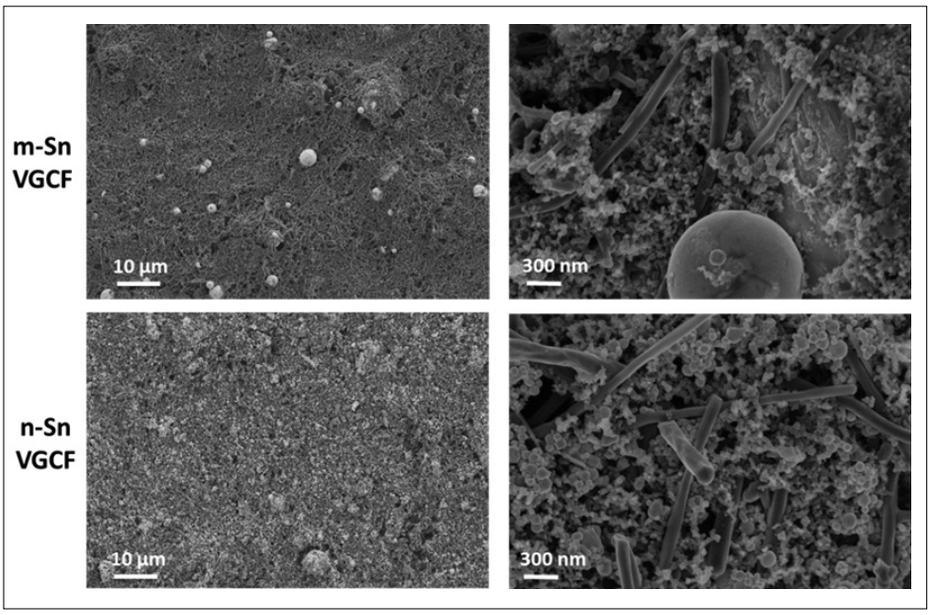

Fig. 4. SEM images of electrode containing VGCF as conductive agent (composition 2) of m-Sn (top) and n-Sn (bottom).

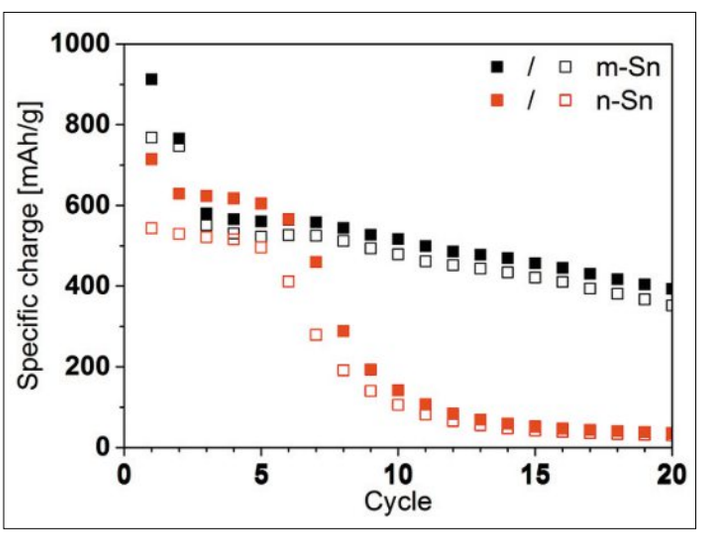

Fig. 5. Cycling Performance obtained with the composition 2.

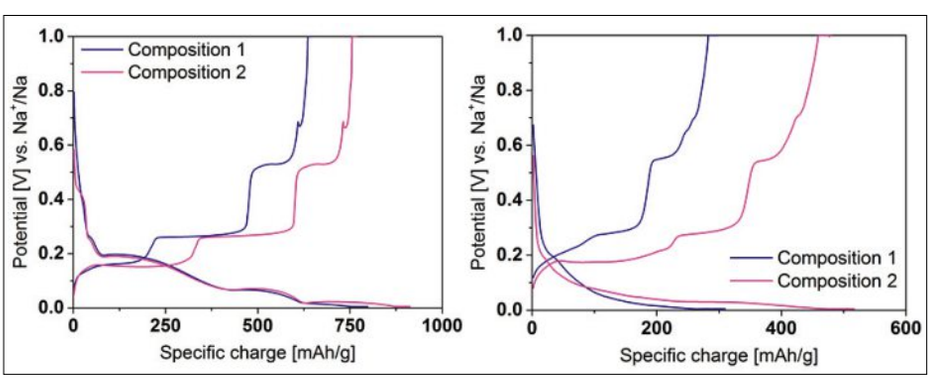

Fig. 6. Galvanostatic curves for the 1st (left) and 10th (right) cycle for m-Sn electrodes using either the composition 1 or the composition 2.

it is much longer. At higher potentials, the last potential plateau at 0.55 V matches for both compositions. These differences in 'length' (*i.e.* specific charge) indicate that VGCF is of great help to maintain the cohesion of m-Sn electrodes during the high volume changes occurring while cycling.

The same analysis was conducted for the n-Sn electrodes, and the galvanostatic curves are plotted and presented in Fig. 7. For the first sodiation the curves match almost perfectly between the two compositions. Only a tiny difference at *ca.* 0.45 V and at 10 mV where the last potential plateau is slightly shorter can be seen. On desodiation we notice that the capacity retention is better for composition 1 than for composition 2 (though only 20–30 mAh/g). After 10 cycles, the specific charge fades dramatically compared to the first cycles. The curves turn smoother compared to the first cycle which makes it difficult to see the different potential plateaux characteristic of the Na-Sn reaction. In both sodiation and desodiation we can see an increase of the polarization for the electrode with composition 2, which can be attributed to a thicker SEI resulting in higher resistance. A thicker SEI can be attributed to the nanoparticles themselves, since their specific area is high and leads to more electrolyte decomposition and when VGCF is present additional SEI formation occurs on its surface. On sodiation, we can notice a small feature at around 0.4 V attributed most probably to the SEI, and then a potential plateau at around 50 mV attributed to the Na-Sn reaction. On desodiation, the different potential plateaus are more visible and look the same for the two systems. Once again the specific charge of the electrode cycled with the composition 2 is lower than the one cycled with the composition 1 due to the observed overpotential.

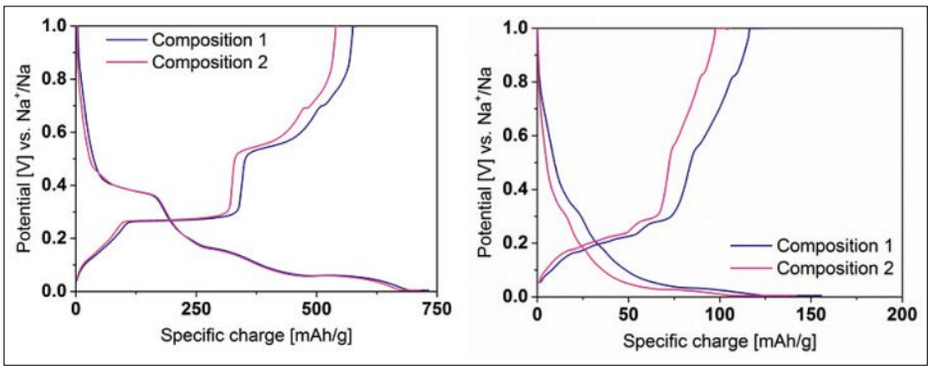

Fig. 7. Galvanostatic curves for the 1st (left) and 10th (right) cycle for n-Sn electrodes using either the composition 1 or the composition 2.

Conclusion

Contrary to the frequent reports of high-performance nanoparticle batteries, we find that nanoparticles offer no long-term advantage compared to micro-sized particles once the electrode loading is the same. Regardless of any electrode engineering, the drawback of the high surface area of nanoparticles and the consequent electrolyte decomposition on this surface cannot be mitigated. For electrodes containing the m-Sn, adding carbon fibers leads to stabilization of the specific charge compared to electrodes without such fibers. This improvement can be traced to the conductive fiber maintaining electrical contact between the active material and the conductive carbon/binder matrix during the volume changes occurring upon cycling. A composition of 70% active material, 12% carboxymethyl cellulose binder, 9% Super C65 and 9% VGCF shows the best electrochemical performance. We thus stress the need for careful electrode engineering already at the stage of fundamental research, to be able to make conclusive statements about how materials and their performances compare.

Acknowledgement

The Swiss National Science Foundation is thanked for financial support (Project 200021_156597). This work was performed within the Swiss Competence Center of Energy Research Heat and Storage (SCCER) framework.

Received: August 8, 2015

[1] T. Oshima, M. Kajita, A. Okuno, *Int. J. Appl. Ceram. Technol.* **2004**, *1*, 269.
[2] V. L. Chevrier, G. Ceder, *J. Electrochem. Soc.* **2011**, *158*, A1011.
[3] M. Dahbi, N. Yabuuchi, K. Kubota, K. Tokiwa, S. Komaba, *PhysChemChemPhys* **2014**, *16*, 15007.
[4] F. Klein, B. Jache, A. Bhide, P. Adelhelm, *PhysChemChemPhys* **2013**, *15*, 15876.
[5] V. Palomares, P. Serras, I. Villaluenga, K. B. Hueso, J. Carretero-Gonzalez, T. Rojo, *Ener. Environ. Sci.* **2012**, *5*, 5884.
[6] M. D. Slater, D. Kim, E. Lee, C. S. Johnson, *Adv. Funct. Mater.* **2013**, *23*, 947.
[7] A. Darwiche, C. Marino, M. T. Sougrati, B. Fraisse, L. Stievano, L. Monconduit, *J. Am. Chem. Soc.* **2012**, *134*, 20805.
[8] A. Darwiche, M. T. Sougrati, B. Fraisse, L. Stievano, L. Monconduit, *Electrochem. Commun.* **2013**, *32*, 18.
[9] M. K. Datta, R. Epur, P. Saha, K. Kadakia, S. K. Park, P. N. Kuma, *J. Power Sources* **2013**, *225*, 316.
[10] L. D. Ellis, T. D. Hatchard, M. N. Obrovac, *J. Electrochem. Soc.* **2012**, *159*, A1801.
[11] Y. Kim, Y. Park, A. Choi, N.-S. Choi, J. Kim, J. Lee, J. H. Ryu, S. M. Oh, K. T. Lee, *Adv. Mater.* **2013**, *25*, 3045.
[12] N. Yabuuchi, M. Kajiyama, J. Iwatate, H. Nishikawa, S. Hitomi, R. Okuyama, R. Usui, Y. Yamada, S. Komaba, *Nature Mater.* **2012**, *11*, 512.
[13] H. Yoshida, N. Yabuuchi, S. Komaba, *Electrochem. Commun.* **2013**, *34*, 60.
[14] N. Yabuuchi, M. Yano, S. Kuze, S. Komaba, *Electrochim. Acta* **2012**, *82*, 296.
[15] N. Yabuuchi, M. Yano, H. Yoshida, S. Kuze, S. Komaba, *J. Electrochem. Soc.* **2013**, *160*, A3131.
[16] N. Yabuuchi, H. Yoshida, S. Komaba, *Electrochem.* **2012**, *80*, 716.
[17] H. Yoshida, N. Yabuuchi, K. Kubota, I. Ikeuchi, A. Garsuch, M. Schulz-Dobrick, S. Komaba, *Chem. Commun*. **2014**, *50*, 3677.
[18] Z. Jian, L. Zhao, H. Pan, Y.-S. Hu, H. Li, W. Chen, L. Chen, *Electrochem. Commun*. **2012**, *14*, 86.
[19] H. Kabbour, D. Coillot, M. Colmont, C. Masquelier, O. Mentre, *J. Am. Chem. Soc.* **2011**, *133*, 11900.
[20] D. Kim, E. Lee, M. Slater, W. Lu, S. Rood, C. S. Johnson, *Electrochem. Commun*. **2012**, *18*, 66.
[21] H. Kim, R. A. Shakoor, C. Park, S. Y. Lim, J.-S. Kim, Y. N. Jo, W. Cho, K. Miyasaka, R. Kahraman, Y. Jung, J. W. Choi, *Adv. Funct. Mater.* **2013**, *23*, 1147.
[22] L. Baggetto, C. A. Bridges, J. C. Jumas, D. R. Mullins, K. J. Carroll, R. A. Meisner, E. J. Crumlin, X. S. Liu, W. L. Yang, G. M. Veith, *J. Mater. Chem. A* **2014**, *2*, 18959.
[23] M. Dahbi, T. Nakano, N. Yabuuchi, T. Ishikawa, K. Kubota, M. Fukunishi, S. Shibahara, J.-Y. Son, Y.-T. Cui, H. Oji, S. Komaba, *Electrochem. Commun.* **2014**, *44*, 66.
[24] S. Komaba, T. Ozeki, N. Yabuuchi, K. Shimomura, *Electrochem.* **2011**, *79*, 6.
[25] J. Li, R. B. Lewis, J. R. Dahn, *Electrochem. Solid State Lett.* **2007**, *10*, A17.
[26] L. Vogt, M. E. Kazzi, E. J. Berg, S. Perez-Villar, P. Novak, C. Villevieille, *Chem. Mater*. **2015**, *27*, 1210.
[27] D. Guy, B. Lestriez, D. Guyomard, *Adv. Mater.* **2004**, *16*, 553.
[28] H. A. Wilhelm, C. Marino, A. Darwiche, P. Soudan, M. Morcrette, L. Monconduit, B. Lestriez, *J. Power Sources* **2015**, *274*, 496.
[29] D. Mazouzi, Z. Karkar, C. R. Hernandez, P. J. Manero, D. Guyomard, L. Roue, B. Lestriez, *J. Power Sources* **2015**, *280*, 533.
[30] S. Komaba, K. Suzuki, N. Kumagai, *Electrochem.* **2002**, *70*, 506.
[31] J. Qian, Y. Chen, L. Wu, Y. Cao, X. Ai, H. Yang, *Chem. Commun.* **2012**, *48*, 7070.
[32] L. Wu, D. Buchholz, D. Bresser, L. G. Chagas, S. Passerini, *J. Power Sources* **2014**, *251*, 379.
[33] L. Wu, X. Hu, J. Qian, F. Pei, F. Wu, R. Mao, X. Ai, H. Yang, Y. Cao, *J. Mater. Chem. A* **2013**, *1*, 7181.
[34] D. H. Nam, T. H. Kim, K. S. Hong, H. S. Kwon, *ACS Nano* **2014**, *8*, 11824.
[35] Y. S. Hu, L. Kienle, Y. G. Guo, J. Maier, *Adv. Mater.* **2006**, *18*, 1421.
[36] S. Komaba, T. Mikumo, A. Ogata, *Electrochem. Commun*. **2008**, *10*, 1276.
[37] S.-T. Myung, N. Takahashi, S. Komaba, C. S. Yoon, Y.-K. Sun, K. Amine, H. Yashiro, *Adv. Funct. Mater.* **2011**, *21*, 3231.
[38] J. W. Wang, X. H. Liu, S. X. Mao, J. Y. Huang, *Nano Lett.* **2012**, *12*, 5897.
[39] L. Xiao, Y. Cao, J. Xiao, W. Wang, L. Kovarik, Z. Nie, J. Liu, *Chem. Commun*. **2012**, *48*, 3321.